East European Journal of Physics. 3. 180-193 (2025)
DOI:10.26565/2312-4334-2025-3-16 ISSN 2312-4334

DARCY-FORCHHEIMER FLOW OF OLDROYD-B NANOFLUID OVER AN INCLINED PLATE WITH EXOTHERMIC CHEMICAL REACTIONS AND BAYESIAN NEURAL NETWORK MODELLING

Gadamsetty Revathi[a]*, M. Rekha[b], P. Srividya Devi[b], B.Ch. Nookaraju[c]
[a]*Department of Mathematics, Gokaraju Rangaraju Institute of Engineering and Technology, Bachupally, Hyderabad – 500090, India*
[b]*Department of EEE, Gokaraju Rangaraju Institute of Engineering and Technology, Bachupally, Hyderabad – 500090, India*
[c]*Department of Mechanical Engineering, Gokaraju Rangaraju Institute of Engineering and Technology, Bachupally, Hyderabad, - 500 090, India*
**Corresponding Author e-mail: grevathi1545@grietcollege.com*
Received May 3, 2025; revised June 12, 2025; accepted July 4, 2025

This study investigates the steady, laminar motion of a non-Newtonian Oldroyd-B nanofluid over an inclined plate, integrating Buongiorno's nanofluid model to account for Brownian motion and thermophoresis. The novel integration of couple stress and Forchheimer inertia in the analysis, coupled with advanced Bayesian-regularized ANN modelling, distinguishes this work. Governing equations are transformed using similarity variables and solved numerically via MATLAB's bvp4c solver. The effects of couple stress, relaxation time, Forchheimer number, thermal radiation, thermophoresis, Brownian motion, and activation energy on velocity, temperature, and concentration profiles are systematically analyzed. Results reveal that couple stress and relaxation time reduce velocity, while thermal radiation and thermophoresis elevate temperature. Brownian motion decreases concentration, and activation energy influences both temperature and concentration oppositely. Multiple linear regression models quantify relationships between friction factor, Nusselt, and Sherwood numbers and key parameters, while a Bayesian-regularized artificial neural network (ANN) demonstrates high predictive accuracy (R-values ~1). It is noticed that increasing the couple stress parameter from 0.1 to 2.5 reduces friction factor by 59.8%, increasing the thermophoresis parameter from 0.1 to 2.5 decreases the Nusselt number by 7.8%, reflecting reduced heat transfer, and increasing the Brownian motion parameter from 0.1 to 2.5 reduces the mass transmission rate by 2.6%.
Keywords: *Non-Newtonian fluid; Thermophoresis; bvp4c; Brownian motion; Activation energy; Thermal radiation*
PACS: 47.15.-x, 47.50.-d

Nomenclature

u, v – the velocity components in the directions of x-axis and y-axis	η – Similarity variable
σ^* – Stefan-Boltzman constant	Nb – Brownian motion parameter
Pr – Prandtl number	C_p – Specific heat capacity
τ – Heat capacity ratio	Λ – Porosity parameter
ν – Kinematic viscosity	Nt – Thermophoresis parameter
g – Acceleration due to gravity	k_r – Chemical reaction parameter
ρ – Density	f – Stream function (ton-dimensional)
γ – Angle of inclination	k_0 – Mean Absorption coefficient
μ – Viscosity of the fluid	λ^* - Parameter due to buoyancy
K – Permeability	D_T – Diffusion coefficient (Thermophoresis)
Fr – Forchheimer number	D_B – Diffusion coefficient (Brownian motion)
k – Thermal conductivity	α – Thermal diffusivity
B_0 – Magnetic strength	α_1 – Temperature ratio parameter
Mg – Magnetic field parameter	m – The fitted rate constant
σ – Electrical conductivity	Γ – Reaction rate parameter (non-dimensional)
λ – Parameter due to Mixed convection	A – Activation energy parameter
	Ra – Radiation parameter

1. INTRODUCTION

Newtonian as well as non-Newtonian fluids are the two main types taken into account in fluid mechanics. The viscosity and flow characteristics of these fluids under shear stress serve as the basis for differentiation. Regardless of the applied shear rate, the viscosity of Newtonian fluids remains constant. For instance, water, fuel, alcohol, and many more substances. Because of their rheological properties, non-Newtonian fluids are helpful in a huge range of industrial and technical purposes. A number of significant studies on non-Newtonian fluid models are documented due to said broader use and applications. Many modellings have been proposed to illustrate the fluid response that the Navier-Stokes model cannot explain. These models are divided into three types: differential, integral, and rate models. Oldroyd's [1] report, which was influenced by Frohlick and Sack's [2] work, established a methodical procedure for creating a viscoelastic fluid modelling that was precisely of rate type, even though it had nothing to do with thermodynamical concerns. Among

Cite as: G. Revathi, M. Rekha, P.S. Devi, B.Ch. Nookaraju, East Eur. J. Phys. 3, 180 (2025), https://doi.org/10.26565/2312-4334-2025-3-16

the several models he presented, the Oldroyd-B fluid modelling was analytically feasible and, more importantly, experimentally supported. It was characterised by three material constants namely, the viscosity, relaxation and retardation time. Oudina et al. [3] provided a study of heat transfer efficiency methods in various enclosures as well as nanofluidic applications. Boudjemline et al. [4] investigated Jeffery-Hamel flow extension and Oldroyd-B nanofluid in an enlarged channel. Yasir et al. [5] scrutinized the unsteady motion of an Oldroyd-B fluid that used energy transmission to form an extendable cylindrical surface. Analytic series convergence was one of their topics. Using Buongiorno's model, they also investigated the characteristics of Brownian motion brought on by nanoparticles. Sun et al. [6] reported the numerical outcomes on the Oldroyd-B motion across a triangular cylinder. This study investigates the flow motion in different orientations. Discussion of magnetic impact in the motion of Oldroyd-B fluid along a semi-vertical plate with absorbing boundary assumptions in another discussion of Liu et al. [7]. Fetecau et al. [8] presented the results for MHD motion of Oldroyd-B fluid by a circular cylinder in a saturated porous region. Munir et al. [8] studied numerically the flow behaviour of Oldroyd-B nanofluid. They also reported the entropy generation through their study. Kang et al. [9] used the characteristics of Brownian movement and thermophoresis in a radiative motion of Oldroyd-B fluid. With the help of non-Fourier heat flux, Ahmed et al. [10] presented the outcomes for chemically reactive Oldroyd-B nanofluid bidirectionally with external heat source. Yasir et al. [12] also discussed the unsteady motion of Oldroyed-B fluid via convectively heated surface.

Industrial applications depend heavily on chemical reactions that release energy as heat. However, most of these chemical reactions can become uncontrollable, which is why scientists and engineers are looking for a very efficient way to achieve this aim while maintaining safety, reaction control, and appropriate heat management. Due to this reason, a good amount of literature found on these reactions. For instance, exploration of endothermic and exothermic chemical reactions in a nanofluid motion over a permeable microchannel by Madhukesh et al. [13]. Impacts of these chemical reactions on the different fluid motions discussed by many authors. Ramesh et al. [14], Agbolade and Fatunmbi [15], Maleque [16], Alarabi et al. [17], Shanmugapriya et al. [18], Oderinu et al. [19] and Khan et al. [20] are few of the many recent studies. The reason behind these investigations is that the exothermic chemical reactions have a major impact on engineering applications such chemical separation, oil separation, and combustion processes that require heat transfer in the presence of nanofluids.

Researchers have lately become interested in the movement of fluid through a porous area and objects of various forms immersed in the porous region. Numerous fields, including applied mathematics, mechanical engineering, geothermal physics, nuclear engineering, bioengineering, and civil engineering, have used it. Some processes that include fluid flow via a porous area include the use of geothermal energy, the casting solidification, flow of blood in arteries or lungs, underground electrical wires, the dispersal of pollutants in aquifers, heat pipes (porous), and chemical catalytic connections. The flow filled in the porous region is widely interpreted using Darcy's law. The effects of high velocity and turbulence in the porous region render Darcy's law inapplicable. Practical impact of this law in a variety of mathematical modellings was discussed by many of the researchers in the past and recent literature. Hayat et al. [21] examined the Darcy-Forchheimer motion along with nonlinear mixed convection. Later Khan [22] studied the forced convective Darcy-Forchheimer motion of hybrid nanofluid through a rotating disk. Revathi et al. [23] proposed a similar modelling for the nanofluid flow via an angled plate together with activation energy and thermal radiation. A similar modelling under Darcy-Forchheimer flow together with chemical reactions has been reported by Rasheed et al. [24] recently. Few more relevant studies in recent literature are listed in [25-31] which describes the modelling of Darcy-Forchheimer motion of the nano/hybrid fluids in addition to a variety of physical constraints.

Motivation from the mentioned works a numerical examination is carried out to drag the consequences for a Darcy-Forchheimer motion of Oldroyd-B nanofluid across an inclined plate with hexothermic chemical reactions on the basis of Bayesian Neural Network modelling. No such reports on this modelling are not yet being discussed by the authors. To fill this research gap, we assumed this type of modelling and presented the numerical outcomes via plots and tables. It means the novel aspect of present investigation is hidden in its formulation. Usage of couple stress, Darcy-Forchheimer and ANN distinguishes from the similar studies. The numerical outcomes are picked out from bvp4c solver in MATLAB. Validation of the results also presented with Bayesian Neural Network.

2. FORMULATION OF THE STUDY

This research focuses on the flow characteristics of a non-Newtonian (Oldroyd B) fluid across an angled upright plate. Assumptions for this study are outlined as below:

- The flow is steady and laminar.
- The plate is inclined at an angle α, with the x −axis along the flow and the y −axis normal to it.
- Buongiorno's nanofluid model is used, incorporating:
    - Brownian motion (nanoparticle diffusion).
    - Thermophoresis (nanoparticle migration due to temperature gradients).
- A uniform magnetic field B is applied vertically (along y −axis).
- The induced magnetic field is negligible (low magnetic Reynolds number).
- Joule heating and Viscous dissipation are omitted.
- No-slip condition at the plate surface.

- The Boussinesq approximation is used for buoyancy effects.
- The chemical reaction is considered to be exothermic, meaning that it releases heat ($\beta > 0$).

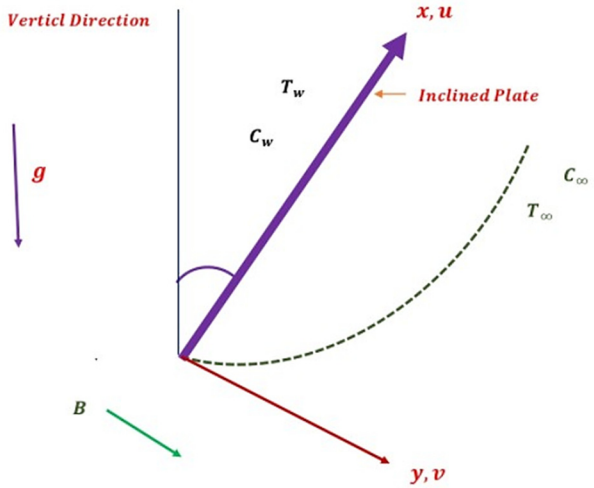

Figure 1. Graphical depiction of the current research

The following conditions and equations are essential for this investigation, based on the previously given assumptions (Singh et al. [32], Muhammad et al. [33], Reddy et al. [34]):

$$\frac{\partial v}{\partial y}+\frac{\partial u}{\partial x}=0 \tag{1}$$

$$\begin{aligned}&\frac{\partial u}{\partial y}v+\frac{\partial u}{\partial x}u=\frac{\partial^2 u}{\partial y^2}\frac{\mu}{\rho}-\delta_1\left(u^2\frac{\partial^2 u}{\partial x^2}+2uv\frac{\partial^2 u}{\partial x\partial y}+v^2\frac{\partial^2 u}{\partial y^2}\right)\\&+\frac{\mu}{\rho}\delta_2\left(u\frac{\partial^3 u}{\partial x\partial y^2}-\frac{\partial u}{\partial x}\frac{\partial^2 u}{\partial y^2}+v\frac{\partial^3 u}{\partial y^3}-\frac{\partial u}{\partial y}\frac{\partial^2 v}{\partial y^2}\right)-\frac{\mu}{\rho}\frac{1}{\kappa}u-B^2u\frac{\sigma}{\rho}-\frac{\gamma_0}{\rho}\frac{\partial^4 u}{\partial y^4}\\&+\left[\beta_T\left(T-T_\infty\right)g+\beta_C\left(C-C_\infty\right)g\right]\mathrm{Cos}\,\alpha-Fu^2\end{aligned} \tag{2}$$

$$\begin{aligned}&\frac{\partial T}{\partial x}u+\frac{\partial T}{\partial y}v=\frac{1}{\left(\rho C_p\right)}\frac{\partial^2 T}{\partial y^2}k+\beta\frac{1}{C_p}k_0^2\left(\frac{T}{T_\infty}\right)^m\exp\left(-\frac{E_0}{k_1T}\right)\left(C-C_\infty\right)\\&+\frac{1}{\left(\rho C_p\right)}\frac{16}{3}\frac{\sigma^*T_\infty^3}{k^*}\frac{\partial^2 T}{\partial y^2}+\tau\left(D_B\frac{\partial T}{\partial y}\frac{\partial C}{\partial y}+\frac{1}{T_\infty}D_T\left(\frac{\partial T}{\partial y}\right)^2\right)\end{aligned} \tag{3}$$

$$v\frac{\partial C}{\partial y}+u\frac{\partial C}{\partial x}=D_B\frac{\partial}{\partial y}\left(\frac{\partial C}{\partial y}\right)+\frac{D_T}{T_\infty}\frac{\partial^2 T}{\partial y^2}-k_0^2\left(\frac{T}{T_\infty}\right)^m\exp\left(-\frac{E_0}{k_1T}\right)\left(C-C_\infty\right) \tag{4}$$

$$\left.\begin{aligned}&C=C_w,v=0,u=0,T=T_w,\frac{\partial^2 u}{\partial y^2}=0,\ \text{at } y=0,\\&C\to C_\infty,u\to 0,T\to T_\infty,\frac{\partial u}{\partial y}\to 0,\text{as y}\to\infty.\end{aligned}\right\} \tag{5}$$

For the purpose of converting regulatory equations, Sudarmozhi et al. [35] introduced further similarity transformations:

$$\left.\begin{aligned}&\eta=\frac{y}{x}Ra_x^{0.25},\ Ra_x=\frac{g\beta_T\left(T_w-T_\infty\right)x^3}{\alpha\upsilon},u=\frac{\alpha}{x}Ra_x^{0.5}f',\\&v=\frac{\alpha}{4x}\eta Ra_x^{0.25}f'-\frac{3\alpha}{4x}Ra_x^{0.25}f,\phi(\eta)=\frac{C-C_\infty}{C_w-C_\infty},T=T_\infty+\theta(\eta)\left(T_w-T_\infty\right).\end{aligned}\right\} \tag{6}$$

Through the use of terms in (6), the continuity equation (1) is satisfied in a straightforward manner. Terms in (6) can then be skilfully used to convert (2 - 5) as the following:

$$\frac{3}{4}ff''-\frac{\Lambda_1}{2}\frac{1}{\sqrt{\Pr}}\left(f'^3+3\eta f'^2 f''+\frac{3}{2}ff'f''+\frac{9}{4}f^2f'''\right)-\frac{f'^2}{2}-\sqrt{\Pr}\left(Mg+\frac{1}{Da}\right)f' \\ +\frac{\Lambda_2}{2}\frac{1}{\sqrt{\Pr}}\left(\frac{f''^2}{2}-f'f'''-\frac{3}{2}ff^{iv}\right)-Frf'^2+\Pr(\theta+\lambda\phi)\cos\alpha-Csf^v=0 \tag{7}$$

$$\left(1+\frac{4}{3}Ra\right)\theta''+\frac{3}{4}f\theta'+\chi\Gamma(1+S\theta)^m\exp\left(-\frac{A}{1+S\theta}\right)\phi+Nb\theta'\phi'+Nt\theta'^2=0 \tag{8}$$

$$\frac{1}{Le}\phi''+\frac{3}{4}f\phi'+\frac{1}{Le}\frac{Nt}{Nb}\theta''-\Gamma(1+S\theta)^m\exp\left(-\frac{A}{1+S\theta}\right)\phi=0 \tag{9}$$

$$\left.\begin{array}{l}\text{at } \eta=0:\phi=1, f=0, f'=0, \theta=1, f'''=0,\\ \text{as } \eta\to\infty:\theta\to0, f''\to0, f'\to0, \phi\to0.\end{array}\right\} \tag{10}$$

where

$$\left.\begin{array}{l}\Pr=\dfrac{\upsilon}{\alpha}, Mg=\sqrt{\dfrac{1}{g\beta_T(T_w-T_\infty)}}\dfrac{\sigma B_0^2}{\rho}, Cs=\sqrt{\dfrac{g\beta_T(T_w-T_\infty)}{\upsilon}}\dfrac{\gamma_1}{\rho\alpha^{3/2}}, \gamma_0=\gamma_1\sqrt{x}, Ra=\dfrac{4\sigma^*T_\infty^3}{kk^*},\\ Da=\dfrac{\kappa_0\sqrt{\alpha g\beta_T(T_w-T_\infty)}}{\upsilon}, \kappa=\kappa_0\sqrt{x}, Fr=\dfrac{C_b}{\sqrt{\kappa}}, \Lambda_1=\delta_0\sqrt{g\beta_T(T_w-T_\infty)}, \delta_0=\dfrac{\delta_1}{\sqrt{x}},\\ Nb=\dfrac{\tau(C_w-C_\infty)D_B}{\alpha}, Le=\dfrac{\alpha}{D_B}, \Gamma=\dfrac{k_r^2}{\alpha}, k_r=k_0x, \Lambda_2=\delta^*\sqrt{g\beta_T(T_w-T_\infty)}, \delta^*=\dfrac{\delta_2}{\sqrt{x}},\\ A=\dfrac{E_0}{k_2T_\infty}, S=\dfrac{T_w-T_\infty}{T_\infty}, Nt=\dfrac{\tau(T_w-T_\infty)D_T}{\alpha T_\infty}.\end{array}\right\}$$

Friction factor, Nusselt and Sherwood numbers are outlined as:

$$\left.\begin{array}{l}Cf=\dfrac{x^2}{\mu\alpha Ra_x}\tau_w\Big|_{y=0}, \tau_w=\mu\dfrac{\partial u}{\partial y},\\ Nu=\dfrac{q_w}{k_f(T_w-T_\infty)}\Big|_{y=0}, q_w=-\left(k_f+\dfrac{16\sigma^*T^3}{3k^*}\right)\left(\dfrac{\partial T}{\partial y}\right),\\ Sh=\dfrac{s_w}{D_B(C_w-C_\infty)}\Big|_{y=0}, s_w=-D_B\left(\dfrac{\partial C}{\partial y}\right).\end{array}\right\} \tag{11}$$

Terms in (6) allows us to rewrite the terms in (11) as

$$\left.\begin{array}{l}(Ra_x)^{\frac{1}{4}}Cf=f''(0),\\ (Ra_x)^{-\frac{1}{4}}Nu=-\left(1+\dfrac{4}{3}Ra\right)\theta'(0),\\ (Ra_x)^{-\frac{1}{4}}Sh=-\phi'(0).\end{array}\right\}$$

3. NUMERICAL PROCEDURE

The transformed governing equations (7 - 9) subject to the restrictions (10) are worked out with the bvp4c solver in MATLAB. This solver is a finite-difference method designed to obtain the solutions of boundary value problems (BVPs) for ordinary differential equations (ODEs) by employing a collocation technique. It adaptively adjusts mesh points to ensure accuracy and efficiency. Advantages include its robustness in handling nonlinear and stiff BVPs, automatic error control for high precision, flexibility with various boundary conditions, and ease of implementation, making it ideal for complex fluid dynamics problems like those in this study.

4. DISCUSSION OF OUTCOMES

This section systematically examines the impacts of key parameters- including couple stress, thermal radiation, thermophoresis, and relaxation time of the fluid- on velocity, temperature, and concentration profiles.

The rise in couple stress within a fluid leads to an increase in internal resistance against deformation, which in turn reduces the fluid's velocity (see Fig. 2). Couple stress arises from micro-rotational effects in complex fluids (e.g., liquid crystals or polymeric fluids), where adjacent fluid elements experience opposing rotational moments. As couple stress increases, these microscopic interactions dissipate more kinetic energy, effectively resisting fluid motion. Physically, this means the fluid exhibits a stronger tendency to resist shear and rotational deformation, resulting in a stiffer response to applied forces and a slower overall flow. This behaviour is particularly relevant in non-Newtonian fluids, where microstructure interactions dominate macroscopic flow properties. Thus, higher couple stress correlates with reduced velocity due to enhanced internal friction and energy dissipation at the microstructural level. In the Oldroyd-B fluid model, the relaxation parameter (Λ_1) represents the time scale over which polymeric stresses in the fluid decay. When Λ_1 increases, the fluid exhibits stronger viscoelastic memory, meaning it retains internal stresses for a longer time, resisting deformation. This increased elastic resistance opposes the flow, effectively reducing the fluid's velocity (see Fig. 3).

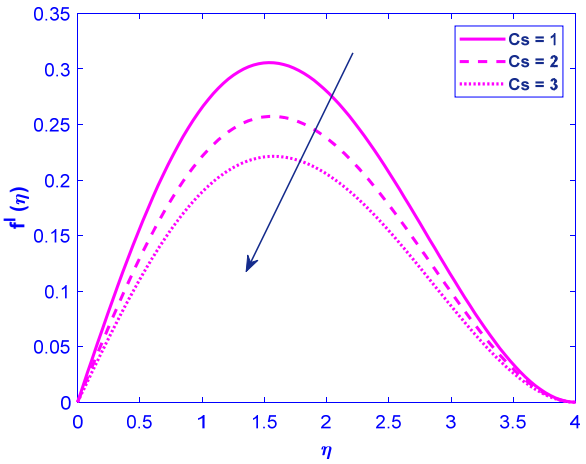

Figure 2. Upshot of Cs on velocity

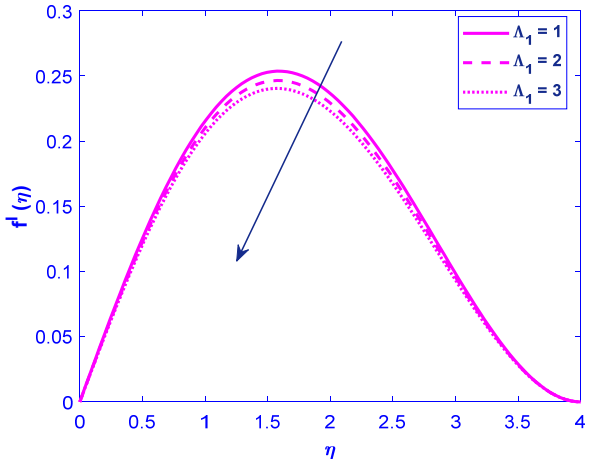

Figure 3. Upshot of Λ_1 on velocity

Physically, this can be interpreted as the polymer chains within the fluid becoming more entangled or stretched, enhancing their ability to store elastic energy and thus dampening momentum transfer. Consequently, a higher Λ_1 leads to a slower velocity profile, as more energy is dissipated through elastic recoil rather than kinetic motion. This behaviour is typical of viscoelastic fluids, where elasticity competes with viscous flow, slowing down the overall movement. The Forchheimer number (Fr) quantifies the relative importance of inertial (non-Darcy) effects compared to viscous (Darcy) effects in porous media flow. A rise in Fr indicates stronger inertial resistance, often due to higher flow velocity, larger pore-scale turbulence, or increased fluid inertia. As Fr increases, the inertial drag force opposing the flow becomes more significant, leading to a reduction in the effective fluid velocity (see Fig. 4). Physically, this occurs because energy is dissipated in overcoming additional resistance caused by eddies, flow separation, and momentum exchange at higher velocities. Thus, the velocity decreases to balance the increased inertial dissipation, maintaining equilibrium in the flow system. This effect is particularly notable in high-velocity flows through coarse or fractured porous media. In an exothermic chemical reaction, the activation energy represents the energy barrier that must be overcome for reactants to form products. When the activation energy increases, the reaction rate typically decreases because fewer molecules possess sufficient energy to surpass this higher barrier. As a result, the rate of heat release from the exothermic reaction slows down, leading to a reduction in the overall temperature of the fluid (see Fig. 5).

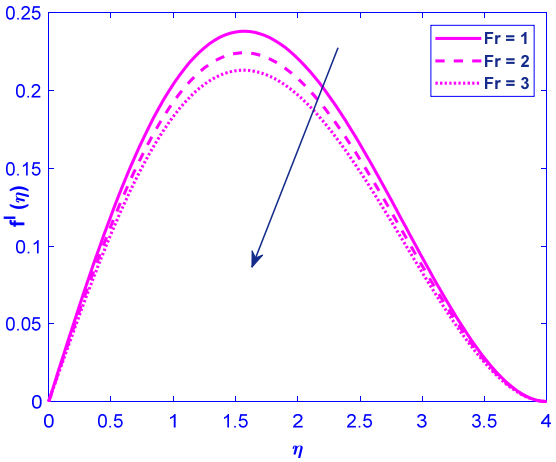

Figure 4. Upshot of Fr on velocity

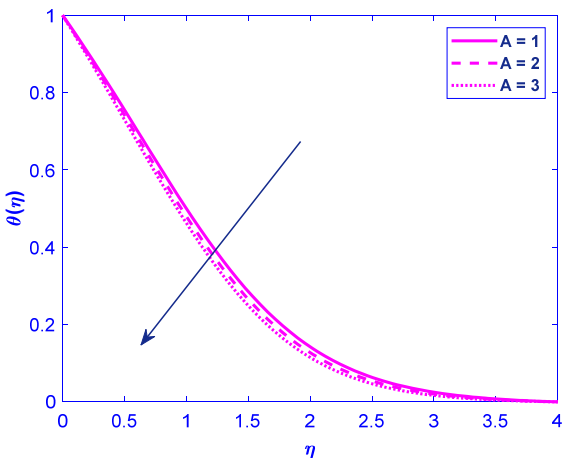

Figure 5. Upshot of A on temperature

Physically, this means that the system generates less thermal energy per unit time because the reaction becomes less efficient at converting reactants into energy-releasing products. The temperature drop reflects the diminished exothermic output due to the higher energy threshold required for the reaction to proceed. The rise in thermal radiation increases the temperature of a fluid because radiation transfers energy in the form of electromagnetic waves, which are absorbed by the fluid's molecules (see Fig. 6). When these waves are absorbed, the molecules gain kinetic energy, leading to increased vibrational and translational motion, which manifests as a rise in temperature. Physically, this process aligns with the first law of thermodynamics, where energy absorption increases the internal energy of the fluid. The extent of heating depends on the fluid's absorptivity—opaque fluids absorb more radiation, converting it efficiently into thermal energy, while transparent fluids may allow radiation to pass through with minimal heating. This mechanism is crucial in applications like solar heating, where radiative energy directly influences fluid temperature. The rise in the thermophoresis parameter increases fluid temperature because thermophoresis involves the migration of particles from hotter to colder regions due to a temperature gradient (see Fig. 7).

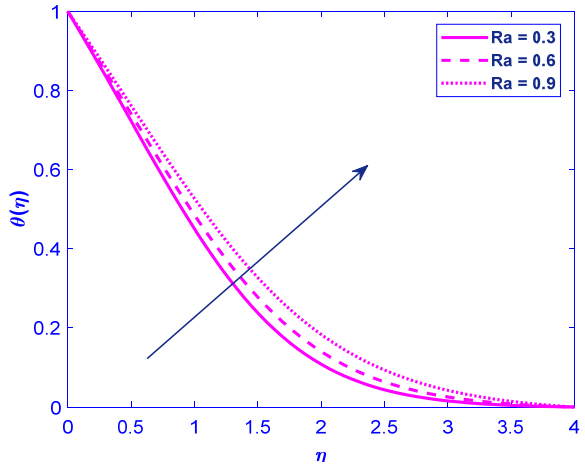

Figure 6. Upshot of Ra on temperature

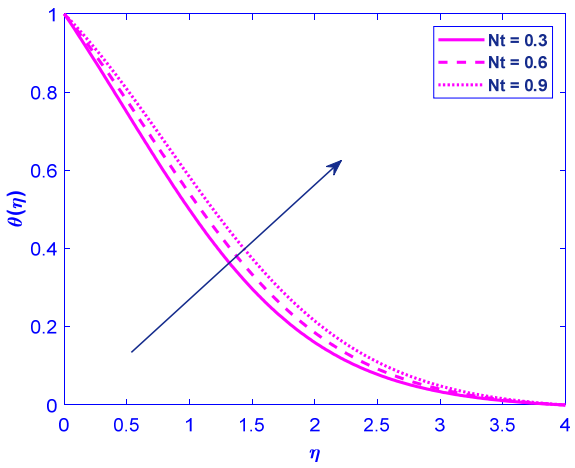

Figure 7. Upshot of Nt on temperature

When the thermophoresis parameter is enhanced, particles move away from the heated surface, carrying thermal energy with them and redistributing it within the fluid. This movement reduces the thermal boundary layer's resistance, allowing more efficient heat transfer into the fluid and elevating its overall temperature. Physically, this phenomenon indicates that stronger thermophoretic effects enhance convective heat transfer by promoting particle-driven energy dispersion, effectively increasing fluid temperature. The result highlights the significant role of particle migration in modifying thermal dynamics, particularly in nanofluids or dusty gases where thermophoresis is prominent. The rise in the Brownian motion parameter enhances the random movement of nanoparticles within a fluid, leading to greater dispersion. As Brownian motion intensifies, nanoparticles spread more uniformly, reducing localized concentration gradients (See Fig. 8). Physically, this means that increased thermal energy drives nanoparticles away from regions of high concentration, promoting mixing and reducing peak fluid concentration. This effect is particularly significant in nanofluids, where enhanced Brownian motion improves heat transfer by distributing particles more evenly, but simultaneously lowers the maximum concentration due to reduced aggregation. Thus, the parameter inversely influences concentration while improving homogeneity. The rise in the activation energy parameter typically increases the fluid concentration because higher activation energy represents a greater energy barrier that molecules must overcome to participate in reactions or diffusion processes (see Fig. 9).

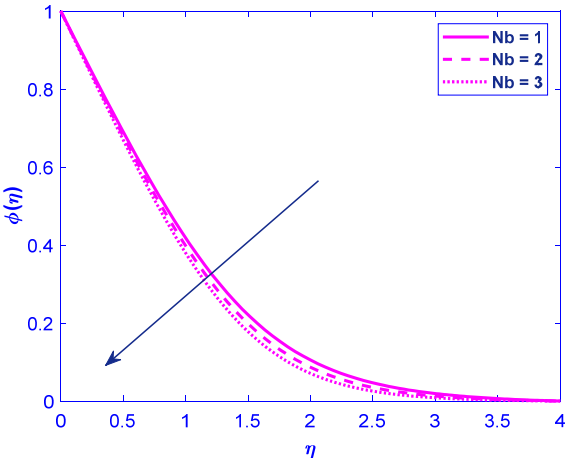

Figure 8. Upshot of Nb on concentration

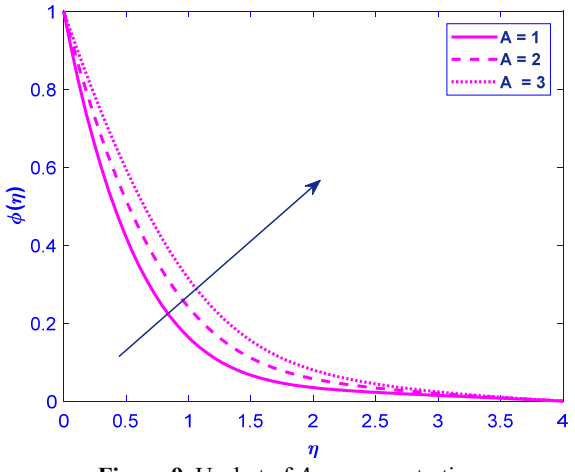

Figure 9. Upshot of A on concentration

When activation energy increases, fewer molecules possess sufficient kinetic energy to react or diffuse, leading to a slower rate of consumption or removal of the fluid species. As a result, the fluid concentration builds up over time since the outflow or reaction rate is reduced. Physically, this implies that systems with higher activation energy tend to retain more of the fluid phase, as the energy threshold restricts dynamic processes like chemical reactions or mass transfer. This effect is particularly relevant in catalysis, combustion, or transport phenomena, where activation energy governs reaction kinetics and species distribution. The increased concentration reflects a bottleneck in molecular activity due to the heightened energy requirement.

4.1. Multiple linear regression

Important technical characteristics, such as the mass transmission rate, and specific variables, such as the Brownian motion, were linked in this study using the models outlined below:

$$Cf = a_0 + a_1\Lambda_1 + a_2 Cs \tag{12}$$

$$Nu = b_0 + b_1 Nt + b_2 A \tag{13}$$

$$Sh = c_0 + c_1 A + c_2 Nb \tag{14}$$

We used 25 different sets of variables for each computation to speed up the process of discovering results:

$$Cf = 2.2124 + 0.0832\Lambda_1 - 0.5199Cs \tag{15}$$

$$Nu = 0.2028 - 0.0784Nt + 0.0568A \tag{16}$$

$$Sh = 0.4264 - 0.0886A + 0.232Nb \tag{17}$$

Equation (15) explains that the friction factor raises with an elevation in Λ_1 and lowers with an increase in Cs. The rise in the couple stress parameter decreases the skin friction coefficient in fluid flow due to the additional resistance to rotational deformation offered by the couple stresses. In fluids with microstructures (e.g., liquid crystals or polymeric fluids), couple stresses account for the resistance to particle rotation, effectively introducing an internal damping mechanism. As the couple stress parameter increases, the fluid's microstructure resists local angular deformations more strongly, reducing the velocity gradient near the boundary. Since skin friction is directly related to the velocity gradient at the wall, a lower gradient results in reduced shear stress and thus a lower skin friction coefficient. Physically, this implies that the fluid's internal microstructure absorbs part of the shear energy, leading to a smoother transition in velocity near the wall and weaker frictional drag. This effect is particularly significant in microfluidic and biological flows where microstructure interactions dominate. The friction factor decreases by 59.8% when the value of Cs ranges from 0.1 to 2.5. Equation (16) demonstrates that the Nusselt number lowers with a spike in Nt and rises with an elevation in A. The rise in the thermophoresis parameter decreases the Nusselt number because thermophoresis causes particles to move from hotter to colder regions, creating a concentration gradient near the heated surface. This particle migration reduces the effective thermal conductivity of the fluid near the boundary, as fewer particles are available to enhance heat transfer. Consequently, the temperature gradient at the wall decreases, leading to a lower Nusselt number, which represents the ratio of convective to conductive heat transfer. Physically, this means that thermophoresis suppresses heat transfer by redistributing particles away from the hot surface, thereby weakening thermal convection. The result highlights the trade-off between particle migration effects and thermal performance in nanofluids. The heat transmission rate diminishes by 7.8% as the value of Nt varies from 0.1 to 2.5. As seen in Equation (17), the Sherwood number decreases as A spikes and increases as Nb climbs. The rise in the Brownian motion parameter enhances the Sherwood number in fluid flow because it intensifies the random motion of nanoparticles, leading to greater mass transfer. Brownian motion increases the dispersion of particles within the fluid, reducing concentration gradients and promoting more uniform mixing. This heightened activity enhances the effective mass diffusivity, thereby improving the convective mass transfer rate, which is quantified by the Sherwood number. Physically, this means that as nanoparticles move more vigorously due to thermal fluctuations, they facilitate faster transport of species across the fluid, increasing the overall mass transfer efficiency. The result highlights the importance of microscopic particle dynamics in macroscopic transport phenomena, particularly in nanofluid applications where enhanced mass transfer is desired. It is observed that as Nb ranges from 0.1 to 2.5, the mass transmission rate drops 2.6%.

4.2 Validation of the results using Artificial Neural Network

In MATLAB, the Bayesian training approach is a regularization method for neural networks that optimizes weights by minimizing a combination of squared errors and weight magnitudes, effectively balancing model complexity and predictive accuracy. This approach treats weights as probabilistic variables, using Bayesian inference to automatically determine optimal regularization parameters, which helps prevent overfitting and improves generalization.

In this study, we rigorously compare our analytical and regression-based results with those generated by a Bayesian-regularized neural network to assess the model's reliability and precision. Our results are exceptionally good, demonstrated by the elevated R-values (approaching 1) in the regression plots (Figs. 10–12), signifying near-perfect correspondence between anticipated and actual values. The error histograms (Figs. 13–15) corroborate this by displaying symmetric, zero-centred distributions with limited dispersion, indicating unbiased and accurate predictions. Furthermore, the function fit plots (Figs. 16–18) illustrate that the neural network effectively represents the fundamental physical trends,

including the inverse relationship between couple stress and skin friction and the positive correlation between Brownian motion and Sherwood number.

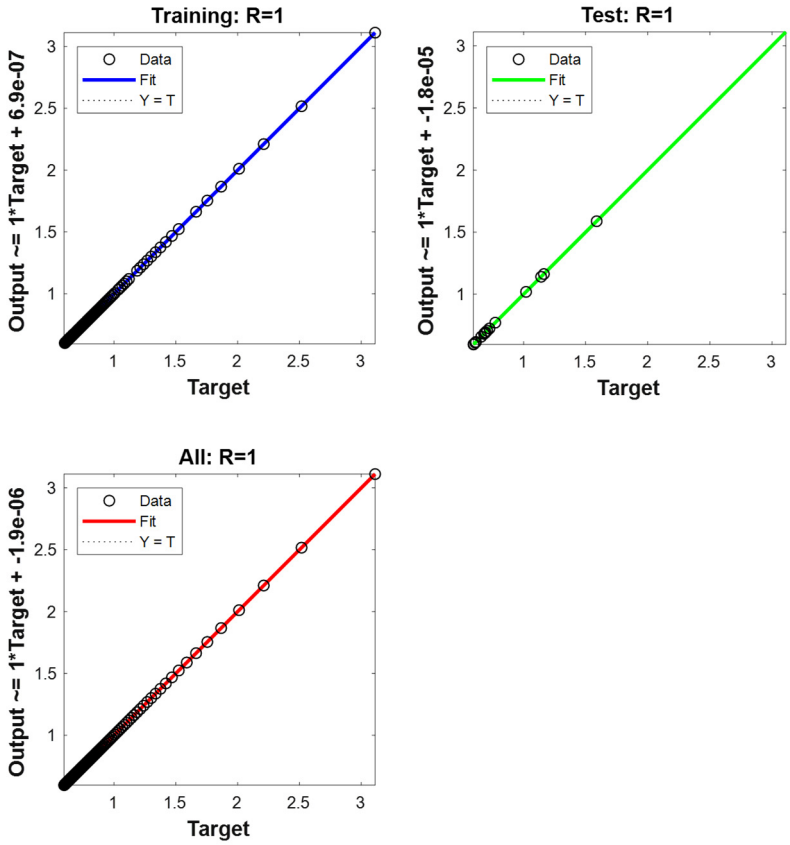

Figure 10. Regression chart for couple stress vs skin friction coefficient

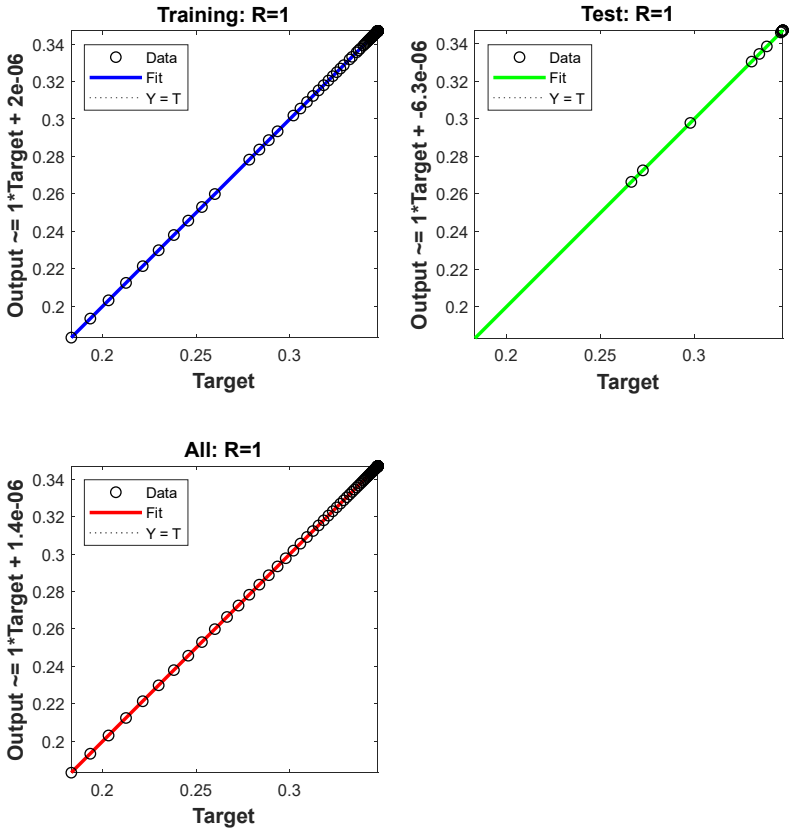

Figure 11. Regression chart for activation energy vs Nusselt number

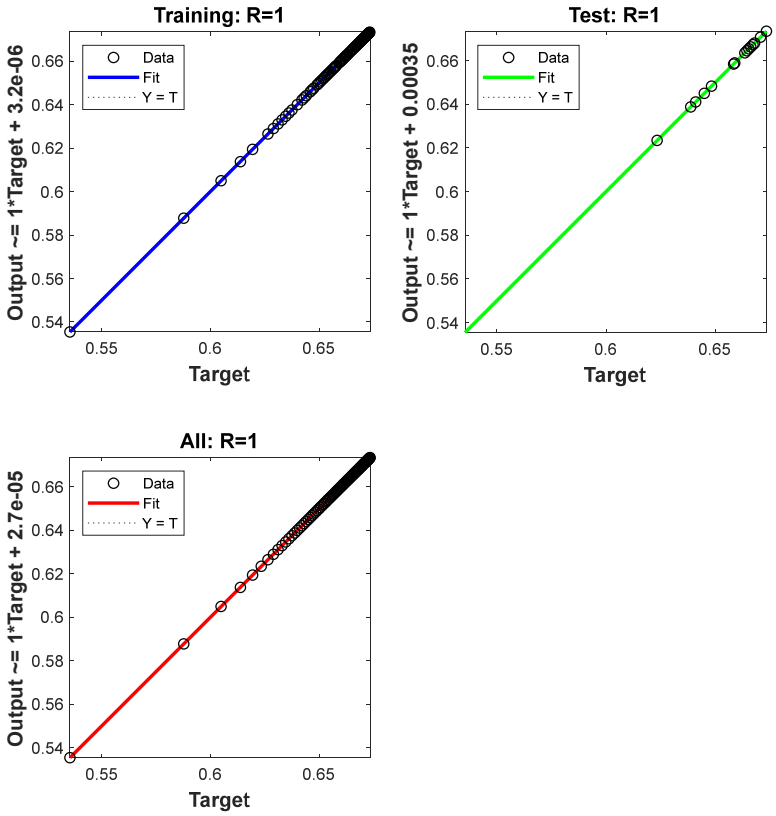

Figure 12. Regression chart for Brownian motion vs Sherwood number

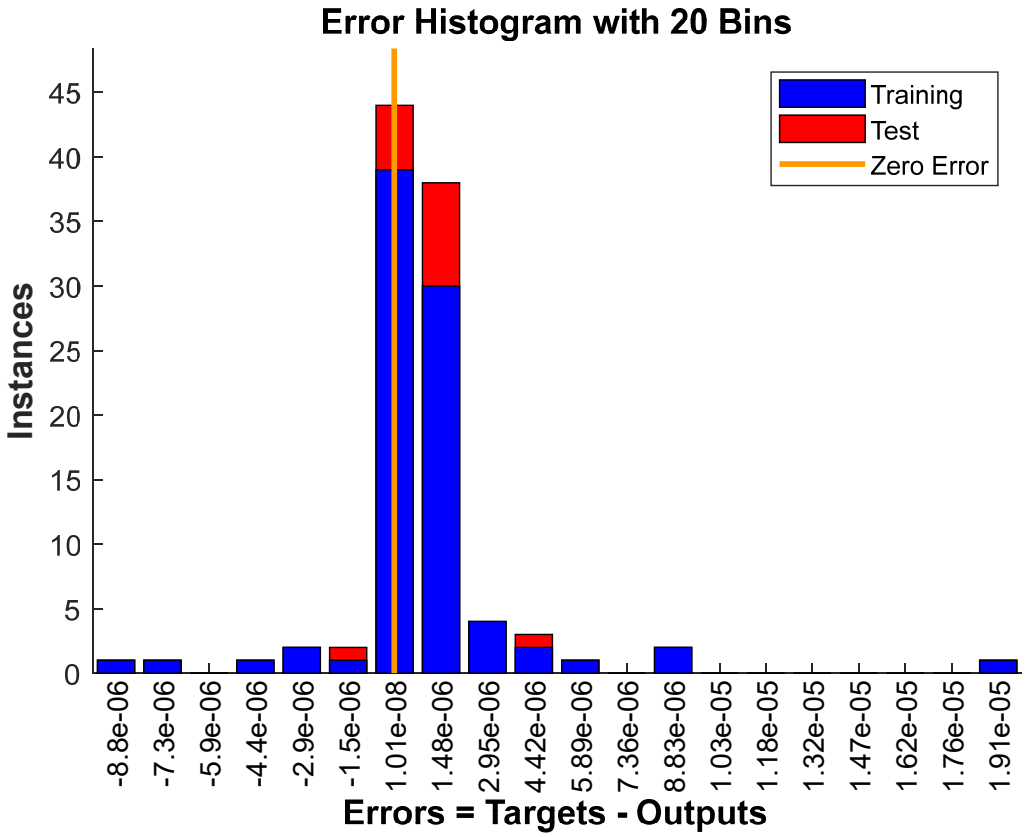

Figure 13. Error histogram for couple stress vs skin friction coefficient

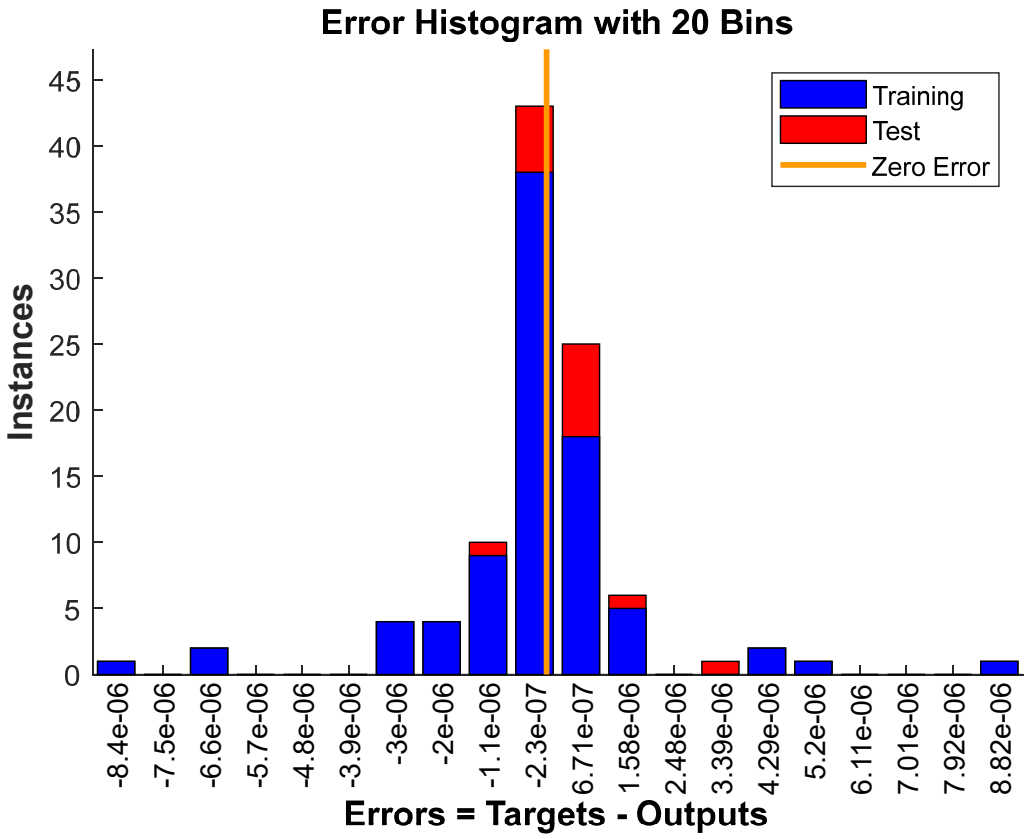

Figure 14. Error histogram for activation energy vs Nusselt number

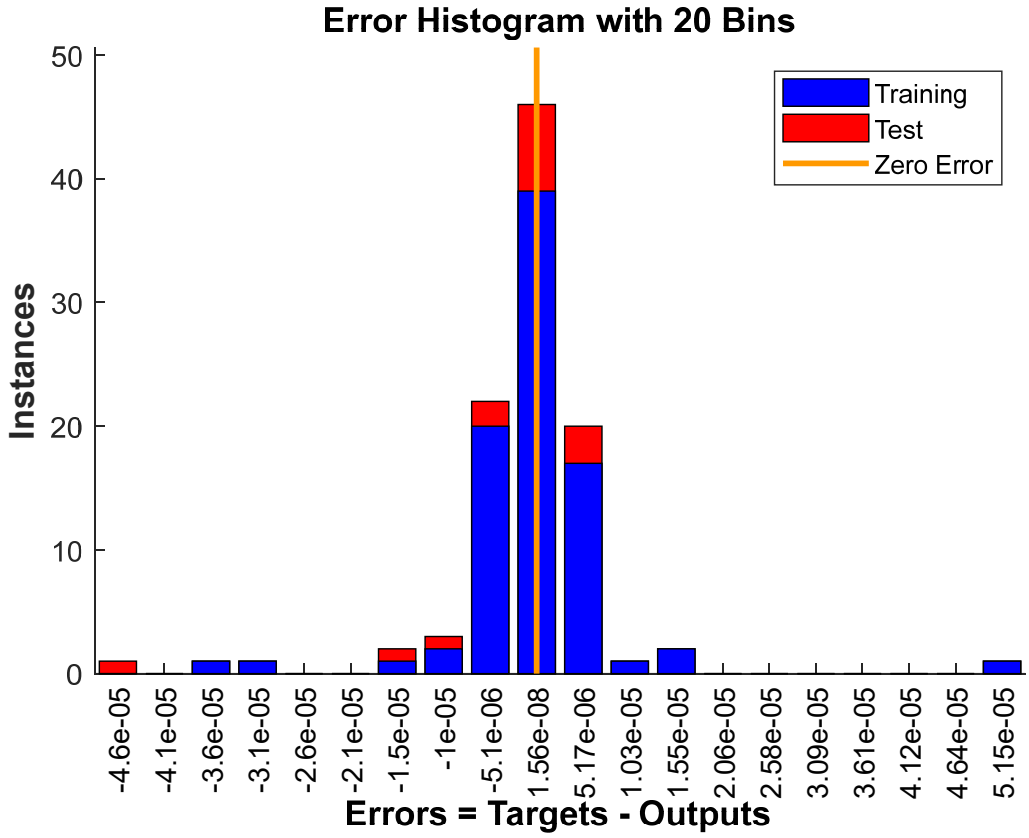

Figure 15. Error histogram for Brownian motion vs Sherwood number

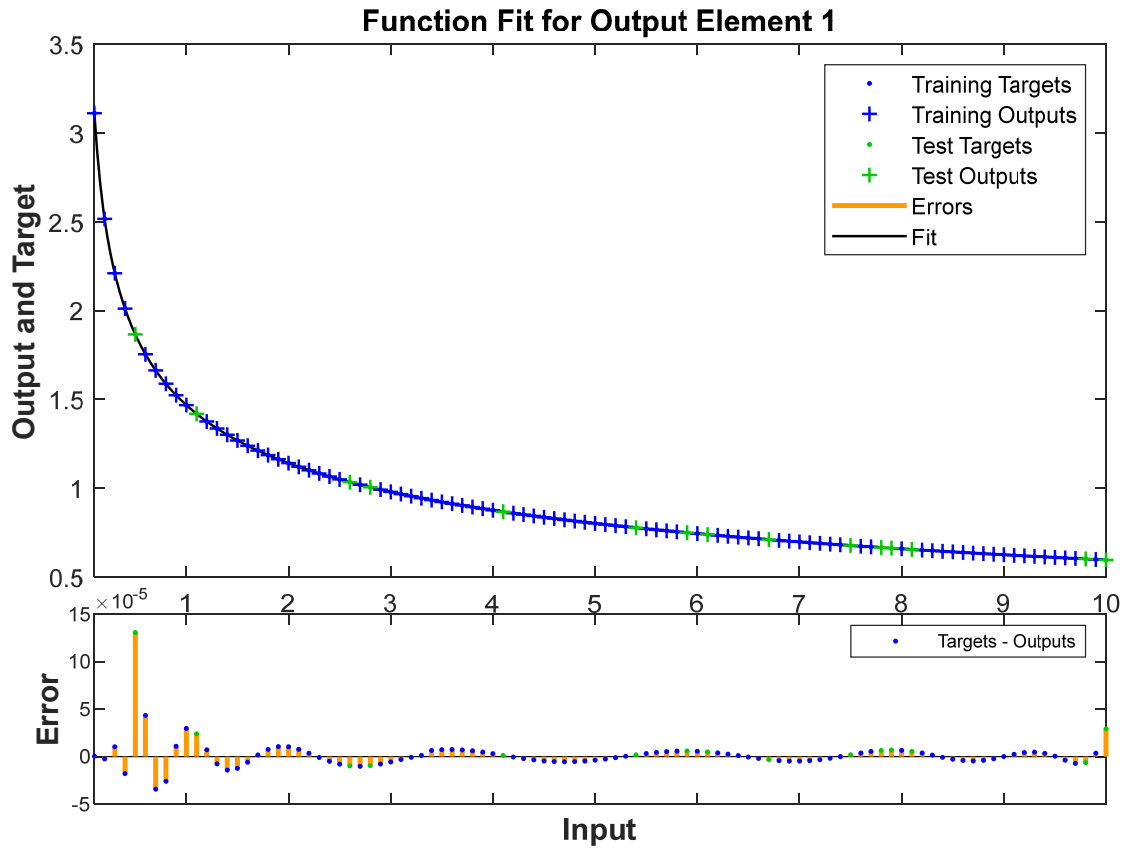

Figure 16. Function Fit plot for couple stress vs skin friction coefficient

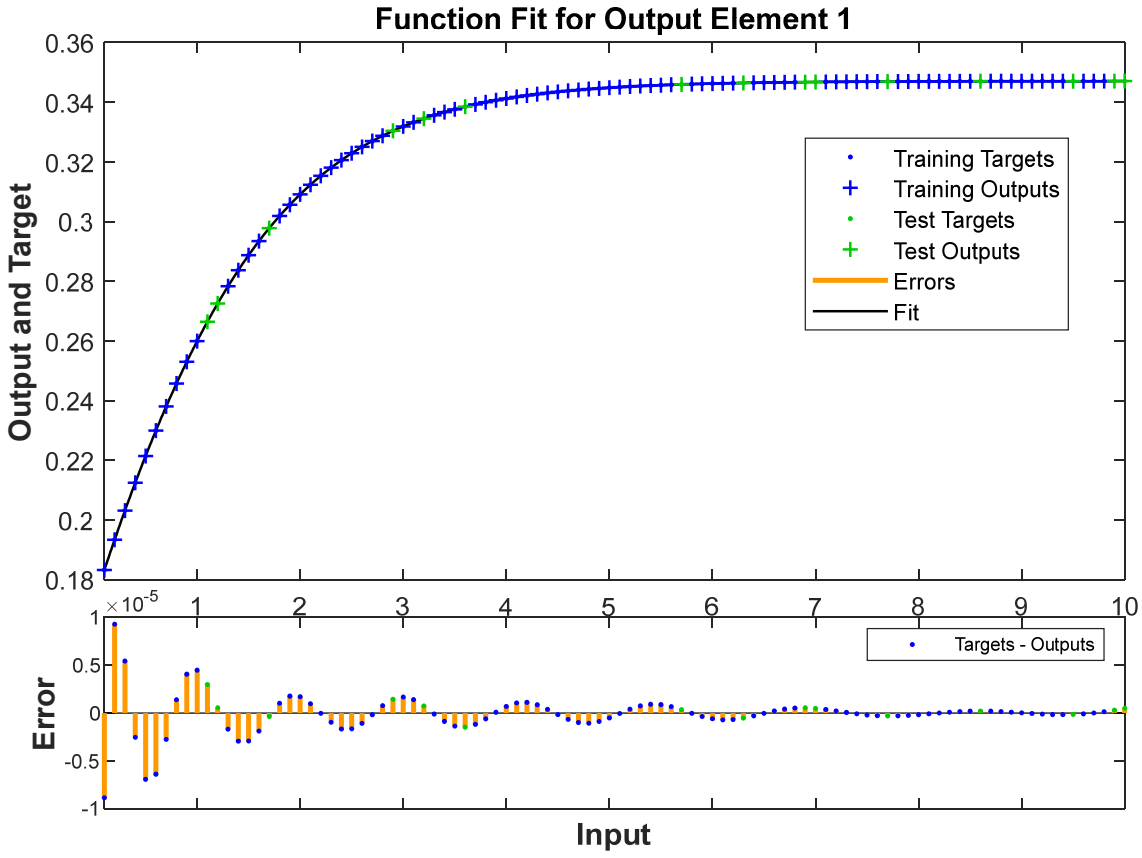

Figure 17. Function Fit plot for activation energy vs Nusselt number

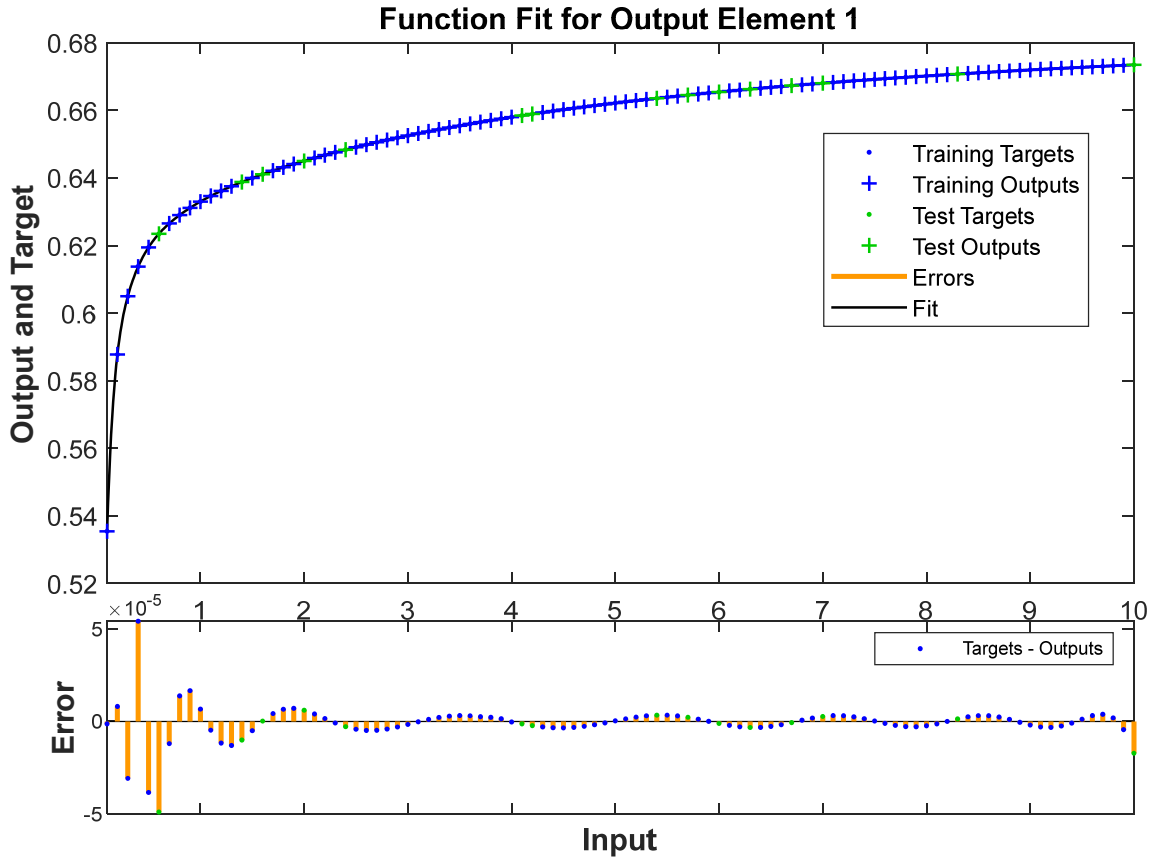

Figure 18. Function Fit plot for Brownian motion vs Sherwood number

5. CONCLUSIONS

This study investigates the steady, laminar motion of a non-Newtonian Oldroyd-B nanofluid across an inclined vertical plate, integrating Buongiorno's nanofluid model to account for Thermophoresis and Brownian motion. The research examines the effects of key parameters such as couple stress, relaxation time, Forchheimer number, thermal radiation, thermophoresis, Brownian motion and the activation energy on velocity, temperature and concentration. Multiple linear regression and a Bayesian-regularized artificial neural network (ANN) are employed to model relationships and predict outcomes, offering insights into complex nanofluid dynamics under viscoelastic, magnetic, and exothermic reaction influences. The findings have applications in heat exchangers, polymer processing, enhanced oil recovery, and biomedical systems. Key findings are mentioned below:

- Increasing couple stress reduces velocity by enhancing viscosity and internal friction.
- Higher relaxation time decreases velocity due to increased fluid elasticity, thickening the boundary layer.
- Higher activation energy decreases temperature by reducing exothermic reaction rates.
- Greater thermophoresis raises temperature through enhanced particle migration from warmer to cooler regions.
- Increased Brownian motion reduces particle concentration by enhancing diffusion.
- Higher activation energy increases concentration by reducing particle mobility.
- It is noticed that increasing the couple stress parameter from 0.1 to 2.5 reduces friction factor by 59.8%.
- Increasing the thermophoresis parameter from 0.1 to 2.5 decreases the Nusselt number by 7.8%, reflecting reduced heat transfer,
- Increasing the Brownian motion parameter from 0.1 to 2.5 reduces the mass transmission rate by 2.6%.
- These findings advance the understanding of complex nanofluid systems and provide robust tools for optimizing engineering applications, such as heat transfer devices, polymer processing, and enhanced oil recovery, where precise control of flow and thermal behaviour is critical.

ORCID

Gadamsetty Revathi, https://orcid.org/0000-0001-9419-2637; **M. Rekha,** https://orcid.org/0000-0001-8842-530X
P. Srividya Devi, https://orcid.org/0000-0001-6131-7421; **B.Ch. Nookaraju,** https://orcid.org/0000-0002-2699-4037

REFERENCES

[1] J.G. Oldroyd, "On the Formulation of Rheological Equations of State," Proceedings of the Royal Society of London. Series A, **200**, 523-541 (1950). https://doi.org/10.1098/rspa.1950.0035

[2] H. Fröhlich and R. Sack, "Theory of the Rheological Properties of Dispersions," Proceedings of the Royal Society of London A, **185**, 415-430 (1946). https://doi.org/10.1098/rspa.1946.0028
[3] F. Mebarek-Oudina and I. Chabani, "Review on nano-fluids applications and heat transfer enhancement techniques in different enclosures," Journal of Nanofluids, **11**(2), 155-168 (2022). https://doi.org/10.1166/jon.2022.1834
[4] A. Boudjemline, I. Ahmad, S. Rehman, Hashim and N. Khedher, "Jeffery-Hamel flow extension and thermal analysis of Oldroyd-B nanofluid in expanding channel," Journal of Non-Equilibrium Thermodynamics, **48**(1), 75-90 (2023). https://doi.org/10.1515/jnet-2022-0052
[5] M. Yasir, A. Ahmed, M. Khan, A.K. Alzahrani, Z.U. Malik and A.M. Alshehri, "Mathematical modelling of unsteady Oldroyd-B fluid flow due to stretchable cylindrical surface with energy transport," Ain Shams Engineering Journal, **14**(1), 101825 (2023). http://dx.doi.org/10.1016/j.asej.2022.101825
[6] F. Sun, X. Wen, X. Si, C. Xie, B. Li, L. Cao, and J. Zhu, "Numerical simulations of the Oldroyd-B fluid flow around triangular cylinders with different orientations," Journal of Non-Newtonian Fluid Mechanics, **326**, 105204 (2024). https://doi.org/10.1016/j.jnnfm.2024.105204
[7] L. Liu, S. Zhang, J. Wang, L. Feng and C. Xie, "Construction of the absorbing boundary condition for the flow of Oldroyd-B fluid over a semi-infinite plate with magnetic effect," Physics of Fluids, **36**(4), 043118 (2024). https://doi.org/10.1063/5.0199911
[8] C. Fetecau and D. Vieru, "Investigating magnetohydrodynamic motions of Oldroyd-B fluids through a circular cylinder filled with porous medium," Processes, **12**(7), 1354 (2024). https://doi.org/10.3390/pr12071354
[9] S. Munir, A. Maqsood, U. Farooq, M. Hussain, M.I. Siddiqui and T. Muhammad, "Numerical analysis of entropy generation in the stagnation point flow of Oldroyd-B nanofluid," Waves in Random and Complex Media, **35**(1), 465-481 (2025). https://doi.org/10.1080/17455030.2021.2023782
[10] L. Kang, B. Khan, S.Z. Abbas, W.A. Khan and S.A. Alrub, "Brownian moment and thermophoresis analysis of nanoparticles for Oldroyd-B fluid capturing aspects of radiation phenomenon," International Journal of Modern Physics B, **39**(12), 2550092 (2025). https://doi.org/10.1142/S0217979225500924
[11] M. Ahmad, S.U. Khan, Q. Bibi, M. Taj and M.M. Bhatti, "Buoyancy-driven bidirectional forced convection in chemically reactive Oldroyd-B nanofluid: incorporating the Cattaneo–Christov model with an external heat source for improved analysis," Particulate Science and Technology, **43**(3), 369-381 (2025). https://doi.org/10.1080/02726351.2025.2457568
[12] M. Yasir, A. Ahmed, M. Khan, M.M.I. Ch and M. Ayub, "Study on time-dependent Oldroyd-B fluid flow over a convectively heated surface with Cattaneo-Christov theory," Waves in Random and Complex Media, **35**(1), 144-161 (2025). https://doi.org/10.1080/17455030.2021.2021316
[13] J.K. Madhukesh, B.C. Prasannakumara, S.A. Shehzad, M.I. Anwar and S. Nasir, "Endothermic and exothermic chemical reactions' influences on a nanofluid flow across a permeable microchannel with a porous medium," International Journal of Ambient Energy, **45**(1), 2325515 (2024). https://doi.org/10.1080/01430750.2024.2325515
[14] G.K. Ramesh, J.K. Madhukesh, E.H. Aly, *et al*., "Endothermic and exothermic chemical reaction on MHD ternary (Fe_2O_4–TiO_2–Ag/H_2O) nanofluid flow over a variable thickness surface," J. Therm. Anal. Calorim. **149**, 6503–6515 (2024). https://doi.org/10.1007/s10973-024-13013-x
[15] O.A. Agbolade and E.O. Fatunmbi, "Thermal explosion and distribution of hydromagnetic Eyring–Prandtl double exothermic diffusion-reaction fluid in a porous channel," Thermal Advances, **1**, 100005 (2024). https://doi.org/10.1016/j.thradv.2024.100005
[16] K.A. Maleque, "Effects of exothermic/endothermic chemical reactions with Arrhenius activation energy on MHD free convection and mass transfer flow in presence of thermal radiation," Journal of Thermodynamics, **2013**(1), 692516 (2013). https://doi.org/10.1155/2013/692516
[17] T.H. Alarabi, S.S. Alzahrani, A. Mahdy and O.A. Abo-Zaid, "Aspects of mass and thermal relaxation time and exothermic chemical processes on the flow of a ternary hybrid Sutterby nanofluid via slant surface with activation energy and linear convection limits," Proceedings of the Institution of Mechanical Engineers, Part E: Journal of Process Mechanical Engineering, 09544089241274054 (2024). https://doi.org/10.1177/09544089241274054
[18] M. Shanmugapriya, R. Sundareswaran, S.G. Krishna and M. Pal, "An analysis of effect of higher order endothermic/exothermic chemical reaction on magnetized Casson hybrid nanofluid flow using fuzzy triangular number," Engineering Applications of Artificial Intelligence, **133**, 108119 (2024). https://doi.org/10.1016/j.engappai.2024.108119
[19] R.A. Oderinu, S.O. Salawu, A.D. Ohaeghue, S. Alao, E.I. Akinola and J.A. Owolabi, "Numerical exploration and thermal criticality of a dual exothermic reaction with radiative heat loss in co-axial cylinder configurations," International Journal of Thermofluids, **25**, 101039 (2025). https://doi.org/10.1016/j.ijft.2024.101039
[20] I. Khan, R. Zulkifli, T. Chinyoka, Z. Ling and M.A. Shah, "Numerical analysis of radiative MHD gravity-driven thin film third-grade fluid flow with exothermic reaction and modified Darcy's law on an inclined plane," Mechanics of Time-Dependent Materials, **29**(1), 1-18 (2025). https://doi.org/10.1007/s11043-024-09744-x
[21] T. Hayat, F. Haider and A. Alsaedi, "Darcy-Forchheimer flow with nonlinear mixed convection," Applied Mathematics and Mechanics, **41**, 1685-1696 (2020). https://doi.org/10.1007/s10483-020-2680-8
[22] M.I. Khan, "Transportation of hybrid nanoparticles in forced convective Darcy-Forchheimer flow by a rotating disk," International Communications in Heat and Mass Transfer, **122**, 105177 (2021). https://doi.org/10.1016/j.icheatmasstransfer.2021.105177
[23] G. Revathi, G. Veeram, M.J. Babu, K.S. Babu and A. Suneel Kumar, "Darcy–Forchheimer flow of power-law (Ostwald-de Waele type) nanofluid over an inclined plate with thermal radiation and activation energy: an irreversibility analysis," International Journal of Ambient Energy, **44**(1), 1980-1989 (2023). https://doi.org/10.1080/01430750.2023.2200434
[24] H.U. Rasheed, W. Khan, M. Kouki, H. Al Garalleh and A. Al Agha, "A mathematical model for three dimensional magnetohydrodynamic thermal nanofluid flow over a permeable Darcy-Forchheimer medium with chemical reaction and activation energy effects," Multiscale and Multidisciplinary Modeling, Experiments and Design, **8**(5), 1-13 (2025). https://doi.org/10.1007/s41939-025-00837-9
[25] F.S. Hira, Q. Rubbab, I. Ahmad and A.H. Majeed, "Advanced computational modeling of Darcy-Forchheimer effects and nanoparticle-enhanced blood flow in stenosed arteries," Engineering Applications of Artificial Intelligence, **152**, 110737 (2025). https://doi.org/10.1016/j.engappai.2025.110737

[26] M. Yasir, M. Naveed Khan, M.A. Abdelmohimen and N.A. Ahammad, "Thermal transport analysis for entropy generated flow of hybrid nanomaterial: modified Cattaneo–Christov heat and Darcy–Forchheimer," Multidiscipline Modeling in Materials and Structures, **21**(2), 291-307 (2025). https://doi.org/10.1108/MMMS-08-2024-0220
[27] N. Khemiri, S. Rehman, T. Saidani and V. Tirth, "Heat transfer analysis of radiated thin-film flow of couple-stress nanofluid embedded in a Darcy-Forchheimer medium with Newtonian heating effects," Nuclear Engineering and Technology, **57**(7), 103510 (2025). https://doi.org/10.1016/j.net.2025.103510
[28] S. Abu Bakar, N.S. Wahid, N.M. Arifin and N.S. Khashi'ie, "The flow of hybrid nanofluid past a permeable shrinking sheet in a Darcy–Forchheimer porous medium with second-order velocity slip," Waves in random and complex media, **35**(1), 46-63 (2025). https://doi.org/10.1080/17455030.2021.2020375
[29] N. Yasin, S. Ahmad, M. Umair, Z. Shah, N. Vrinceanu and G. Alhawael, "Investigations of conjugate heat transfer and fluid flow in partitioned porous cavity using Darcy-Forchheimer model: Finite element-based computations," Case Studies in Thermal Engineering, **72**, 106252 (2025). https://doi.org/10.1016/j.csite.2025.106252
[30] D. Mohanty, G. Mahanta, A.J. Chamkha and S. Shaw, "Numerical analysis of interfacial nanolayer thickness on Darcy-Forchheimer Casson hybrid nanofluid flow over a moving needle with Cattaneo-Christov dual flux," Numerical Heat Transfer, Part A: Applications, **86**(3), 399-423 (2025). https://doi.org/10.1080/10407782.2023.2263906
[31] W. Alghamdi and T. Gul, "Darcy–Forchheimer hybrid nanofluid flow in a squeezing inclined channel for drug delivery applications by means of artificial neural network,"Multidiscipline Modeling in Materials and Structures, **21**(2), 387-404 (2025). https://doi.org/10.1108/MMMS-07-2024-0202
[32] V. Singh, N.B. Naduvinamani, K. Vinutha, B.C. Prasannakumara, J.K. Madhukesh and A. Abdulrahman, "Sodium alginate-based MHD ternary nanofluid flow across a cone and wedge with exothermic/endothermic chemical reactions: A numerical study," Numerical Heat Transfer, Part A: Applications, 1-20 (2024). https://doi.org/10.1080/10407782.2024.2355520
[33] T. Muhammad, A. Alsaedi, T. Hayat and S.A. Shehzad, "A revised model for Darcy-Forchheimer three-dimensional flow of nanofluid subject to convective boundary condition," Results in physics, 7, 2791-2797 (2017). https://doi.org/10.1016/j.rinp.2017.07.052
[34] P.S. Reddy, A.J. Chamkha and A. Al-Mudhaf, "MHD heat and mass transfer flow of a nanofluid over an inclined vertical porous plate with radiation and heat generation/absorption," Advanced Powder Technology, **28**(3), 1008-1017 (2017). https://doi.org/10.1016/j.apt.2017.01.005
[35] K. Sudarmozhi, D. Iranian, I. Khan, A.S. Al-Johani and S.M. Eldin, "Magneto radiative and heat convective flow boundary layer in Maxwell fluid across a porous inclined vertical plate," Scientific Reports, **13**(1), 6253 (2023). https://doi.org/10.1038/s41598-023-33477-5

ПОТІК ДАРСІ-ФОРХГАЙМЕРА ОЛДРОЙД-В НАНОРІДИНИ НАД ПОХИЛОЮ ПЛАСТИНКОЮ З ЕКЗОТЕРМІЧНИМИ ХІМІЧНИМИ РЕАКЦІЯМИ ТА МОДЕЛЮВАННЯМ БАЄСІВСЬКОЮ НЕЙРОННОЮ МЕРЕЖЕЮ

Гадамсетті Реваті[a], М. Рекха[b], П. Шрівідья Деві[b], В.Ч. Нукараджу[c]
[a]Кафедра математики, Інженерно-технологічний інститут Гокараджу Рангараджу, Бачупаллі, Хайдерабад – 500090, Індія
[b]Кафедра електротехніки та електроніки, Інженерно-технологічний інститут Гокараджу Рангараджу, Бачупаллі, Хайдерабад – 500090, Індія
[c]Кафедра машинобудування, Інженерно-технологічний інститут Гокараджу Рангараджу, Бачупаллі, Хайдерабад, - 500 090, Індія

Це дослідження досліджує стаціонарний ламінарний рух неньютонівської нанорідини Олдройда-Б над похилою пластиною, інтегруючи модель нанорідини Буонджорно для врахування броунівського руху та термофорезу. Нова інтеграція парних напружень та інерції Форхгеймера в аналізі, у поєднанні з удосконаленим байєсівсько-регуляризованим моделюванням штучних нейронних мереж, відрізняє цю роботу. Керівні рівняння трансформуються за допомогою змінних подібності та розв'язуються чисельно за допомогою розв'язувача bvp4c у MATLAB. Систематично проаналізовано вплив парного напруження, часу релаксації, числа Форхгеймера, теплового випромінювання, термофорезу, броунівського руху та енергії активації на профілі швидкості, температури та концентрації. Результати показують, що парне напруження та час релаксації зменшують швидкість, тоді як теплове випромінювання та термофорез підвищують температуру. Броунівський рух зменшує концентрацію, а енергія активації впливає як на температуру, так і на концентрацію протилежно. Моделі множинної лінійної регресії кількісно визначають зв'язки між коефіцієнтом тертя, числами Нуссельта та Шервуда і ключовими параметрами, тоді як байєсівсько-регуляризована штучна нейронна мережа (ШНМ) демонструє високу прогностичну точність (значення R ~1). Помічено, що збільшення параметра парного напруження з 0,1 до 2,5 зменшує коефіцієнт тертя на 59,8%, збільшення параметра термофорезу з 0,1 до 2,5 зменшує число Нуссельта на 7,8%, що відображає зменшення теплопередачі, а збільшення параметра броунівського руху з 0,1 до 2,5 зменшує швидкість передачі маси на 2,6%.

Ключові слова: *неньютонівська рідина; термофорез; bvp4c; броунівський рух; енергія активації; теплове випромінювання*